

Returning to the Fold for Lessons in Mitochondrial Crista Diversity and Evolution

Tomáš Pánek^{1,3}, Marek Eliáš¹, Marie Vancová², Julius Lukeš², and Hassan Hashimi^{2,*}

¹Department of Biology and Ecology, Faculty of Science, University of Ostrava, Ostrava 710 00, Czech Republic

²Institute of Parasitology, Biology Center, Czech Academy of Sciences and Faculty of Science, University of South Bohemia, České Budějovice 370 05, Czech Republic

³Present address: Department of Zoology, Faculty of Science, Charles University, Prague 128 43, Czech Republic

*Correspondence: hassan@paru.cas.cz

<https://doi.org/10.1016/j.cub.2020.02.053>

Cristae are infoldings of the mitochondrial inner membrane jutting into the organelle's innermost compartment from narrow stems at their base called crista junctions. They are emblematic of aerobic mitochondria, being the fabric for the molecular machinery driving cellular respiration. Electron microscopy revealed that diverse eukaryotes possess cristae of different shapes. Yet, crista diversity has not been systematically examined in light of our current knowledge about eukaryotic evolution. Since crista form and function are intricately linked, we take a holistic view of factors that may underlie both crista diversity and the adherence of cristae to a recognizable form. Based on electron micrographs of 226 species from all major lineages, we propose a rational crista classification system that postulates cristae as variations of two general morphotypes: flat and tubulo-vesicular. The latter is most prevalent and likely ancestral, but both morphotypes are found interspersed throughout the eukaryotic tree. In contrast, crista junctions are remarkably conserved, supporting their proposed role as diffusion barriers that sequester crista contents. Since cardiolipin, ATP synthase dimers, the MICOS complex, and dynamin-like Opa1/Mgm1 are known to be involved in shaping cristae, we examined their variation in the context of crista diversity. Moreover, we have identified both commonalities and differences that may collectively be manifested as diverse variations of crista form and function.

Introduction

Mitochondria originated from an alphaproteobacterial endosymbiont acquired by a host related to Asgard archaea during eukaryogenesis [1,2]. A vestige of this origin is the presence of two bounding membranes: the outer membrane and inner membrane (Figure 1), descendants of the endosymbiont outer and cytoplasmic membranes, respectively [3]. The double membrane delineates two internal compartments: the intermembrane space between the outer and inner membranes, plus the matrix, which is enveloped by the inner membrane. Most of the inner membrane is usually contained within cristae, infoldings of the membrane that extend into the matrix, whereas the 'inner boundary membrane' represents the part of the inner membrane excluded from cristae.

Cristae are the ultrastructural hallmarks of aerobic mitochondria because they are the framework for respiratory-chain protein complexes, which work in concert to produce ATP by oxidative phosphorylation [4–7]. The respiratory chain's lone soluble electron carrier cytochrome *c* is mostly encapsulated within crista lumina (Figure 1), expediting its electron shuttling between the crista-membrane-embedded complexes III (cytochrome *c* reductase) and IV (cytochrome *c* oxidase) [8]. Moreover, cristae are a platform for the lateral flow of protons pumped into the lumen by complexes I (NADH:ubiquinone oxidoreductase), III and IV to their sink, complex V (F₁F₀-ATP synthase), which utilizes this pH gradient for ATP generation [9]. Thus, cristae are typically absent from the mitochondrion-related organelles of obligate anaerobes, such as the intestinal pathogens *Giardia lamblia* and *Entamoeba histolytica*.

Retention of mitochondrion-related organelles in such lineages documents that mitochondria also play other roles, such as the biogenesis of iron-sulfur clusters, essential enzymatic cofactors [10].

Although cristae are a unifying feature of aerobic mitochondria, they exhibit variations not just between diverse eukaryotes but even within different tissues [11,12]. These conspicuous crista shapes were initially proposed to be suitable characters for large-scale classification of eukaryotes [13–16]. However, according to the current consensual tree of eukaryotes established by phylogenomics, specific crista morphotypes do not define any major well-supported clade. Although several studies have summarized data on crista morphology in the pre-genomics age [17], none has really addressed this issue in light of our current understanding of both eukaryotic evolution and crista-shaping molecules. Distribution of crista-shaping proteins is not correlated with any crista morphotype [18,19]. However, revealing such an interconnection is complicated by the haphazard way many cristae were annotated and a lack of a unified nomenclature for classifying crista morphotypes.

The intention of this review is to take a holistic view of how cristae have been shaped during the evolution of eukaryotes. This entails three tasks: classification of crista shapes based on a comprehensive survey of electron microscopy images from all major eukaryotic lineages, mapping of these shapes onto the current consensus eukaryotic tree, and finally, discussing whether any of the known crista-shaping molecules may underlie this diversity.



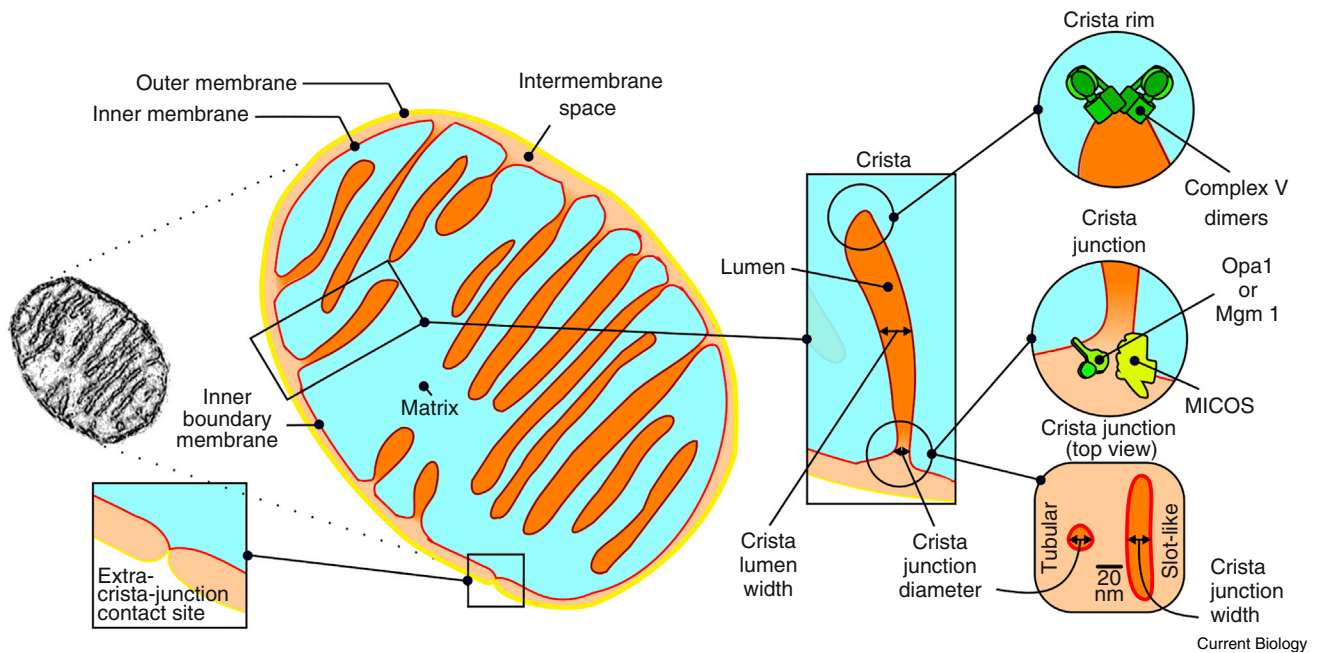


Figure 1. Typical architecture of a mitochondrion.

From left to right, section of three-dimensional reconstructed mitochondrion (adapted from [24]) that is the basis of the main scheme in the middle. The various compartments are labelled. The enrichment of cytochrome *c* is indicated by the darker orange color in the crista lumen, as compared to the lighter shade in the intermembrane space. Similarly, the higher density of respiratory complexes I, III, IV and V in crista membranes is indicated by the dark red color. A contact site between the inner and outer membranes, specifically, one occurring away from a crista junction (labeled here as an ‘extra-crista-junction contact site’), and crista from the schema are highlighted in boxes. The crista junctions and rims are further elaborated in circles, which depict protein complexes discussed in this review. A top view of two crista junction morphologies (viewed from the matrix side) is depicted in the rounded square (bottom right).

A View of the Basic Architecture of Cristae

The golden age of transmission electron microscopy (TEM) in the mid-20th century allowed biologists to peer into cells at upper to mid nanoscales. This allowed Palade and Sjöstrand to observe cristae for the first time, although they did not agree whether they were a baffle of internal ridges within the inner membrane [20] or detached septa dividing the matrix [21] (for historical perspective see [22,23]). The tenuous extrapolation of two-dimensional data from TEM-imaged ultrathin sections to describe a three-dimensional shape led to the discrepancy in their interpretations.

The 1990s saw implementation of electron tomography, allowing detailed three-dimensional reconstruction of cellular ultrastructures at nanometer resolution. This revealed the standard crista architecture [22,23], showing that cristae are attached to the inner boundary membrane by narrow stems called crista junctions, whose diameters are usually less than the crista lumen width (Figure 1) [22–25]. Crista junctions were soon proposed to be diffusion barriers [25], sequestering cytochrome *c* in the lumen [8] and oxidative-phosphorylation protein complexes within the crista membrane [4–7].

This standard crista architecture, sometimes called the ‘crista junction model’ [11], has been consistently observed in ~60 different electron-tomography studies. Abrupt negative membrane curvature occurs at constricted crista junctions, allowing cristae to extend perpendicularly from the inner boundary membrane into the matrix. Following crista junctions are relatively flat regions that terminate at crista rims, sites of positive membrane curvature (Figure 1). However, the vast majority of electron

tomography studies were performed on metazoans and yeast (Figure S1A), both belonging to the supergroup Opisthokonta [26]. The smattering of cristae from outside this group to have been observed by electron tomography almost always conform to the crista junction model. Nonetheless, the ciliate *Paramecium* has tubular cristae attached to the inner boundary membrane at both ends by unconstricted crista junctions [27], indicating that more non-opisthokont cristae should be assessed to test both the prevalence of the crista junction model throughout eukaryotes and the possible existence of alternative crista architectures.

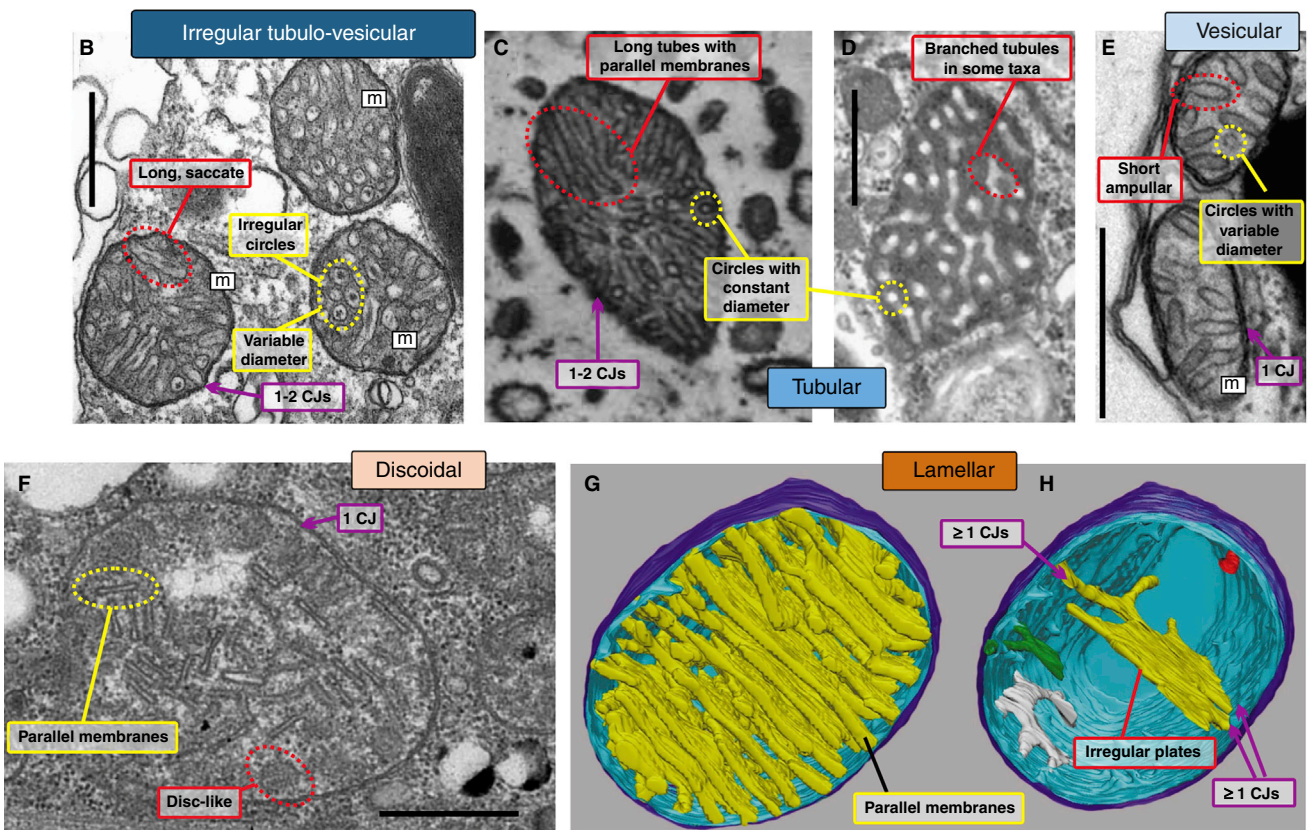
Cristae Are Diverse

Cristae assume various shapes in different eukaryotic lineages. Ensuing representations provided by electron tomography revealed that crista junctions at the base of cristae are not uniform. Most crista junctions were reported to have a tubular morphology, whereas a second type of flattened, slot-like crista junction was observed predominantly in ascomycete fungi and one plant (Figure S1B, Table S1). The occurrence of these two crista-junction morphologies appears to be mutually exclusive, except in the bread mold *Neurospora crassa* [28], human fibroblasts [29] and (presumably) young mouse heart [30].

Although cristae exhibit two major crista-junction morphotypes with similar diameters or widths (see Supplemental Information), the various cristae observed throughout eukaryotes differ in the number of crista junctions they have at their base, in addition to assuming diverse shapes. To get a better grasp

A

	Morphotype	Cross-section	Longitudinal section	Three-dimensional appearance	Crista junctions	Electron tomography study
Tubulo-vesicular	Irregular tubulo-vesicular			Long, saccate	1–2	<i>Polytomella</i> [71]
	Tubular			Long tubules	1–2*	<i>Paramecium</i> [27]
	Vesicular			Short; blob-like or ampullar	1?	Not assigned
Flat	Discoidal			Disc-like; often pedicellate	1	<i>Trypanosoma</i> [83]
	Lamellar			Plate-like or ribbon-like	≥ 1	Chick cerebellum [148]



Current Biology

Figure 2. The menagerie of different crista morphotypes in eukaryotes.

(A) Basic characteristics of each morphotype. (B–E) Transmission electron microscopy images of mitochondria (m) with a range of crista morphotypes. Yellow boxes highlight typical characteristics of cristae in cross-section; red boxes highlight typical characteristics of cristae in longitudinal section. The number of crista junctions (CJ) per crista are shown in purple boxes, but note that the number of crista junctions in branched tubular cristae can be higher. All scale bars = 500 nm. (B) Irregular tubulo-vesicular cristae of a male gamete of the brown alga *Ectocarpus siliculosus*; adapted from [144]. (C) Tubular cristae of the ciliate *Spirostomum ambiguum*; adapted from [145]. (D) Tubular cristae (branched) of the amoebozoan *Flamella arnhemensis*; adapted from [142]. (E) Vesicular cristae of the alveolate

(legend continued on next page)

on this diversity, we have revamped a crista-morphotype classification system proposed in 1993 [17], augmenting it with data generated subsequently. Accordingly, a detailed visual reexamination of TEM images of mitochondrial cristae from 226 species representing all major eukaryotic lineages was undertaken. Their characteristics and typical appearance under TEM are summarized in Figure 2, Table S2, and the Supplemental Information.

We recognize two categories of cristae imaged by TEM as cross-sections: flat and tubulo-vesicular, the latter of which appear circular in the transverse plane (Figure 1). These two categories contain five widely distributed morphotypes: flat cristae assume discoidal and lamellar shapes, whereas tubulo-vesicular cristae can be tubular, vesicular and irregular tubulo-vesicular (Figure 2). Four of these morphotypes have already been broadly recognized [17,18]; the irregular tubulo-vesicular crista subtype is established here.

Artefacts due to sample processing may represent a limitation of the crista classification proposed here, especially given its reliance on TEM images obtained from chemically fixed specimens. This kind of fixation does not stop dynamic activities instantly and may even promote vesiculation in membranous organelles. However, we believe that the proposed crista classification system is on solid ground because sample processing may rather insignificantly affect crista morphology (see Supplemental Information). Furthermore, crista shapes extrapolated from TEM have been often verified by subsequent electron tomography [27,31–33].

Cristae Are Dynamic

Cristae are not static, and imaging may only capture one of many shapes these structures can assume *in vivo*. Pioneering work demonstrated that mitochondrial morphology is dynamic, directly influenced by the organelle's physiological state [34]. When respiration of isolated mitochondria is artificially accelerated by a molar excess of ADP and P_i , the organelle assumes a 'condensed' appearance: the matrix contracts while both the intermembrane space and crista lumen swell. Upon depletion of ADP and P_i , mitochondria assume an 'orthodox' appearance, which is typically observed *in situ* under normal physiological conditions. Thus, crista shape can be a manifestation of the respiratory state of the mitochondrion. Indeed, cristae remodeling affects how individual oxidative phosphorylation complexes are configured into supercomplexes, which can in turn influence the respiratory chain's bioenergetic flux [35].

Cristae can be deliberately remodeled. Bloodborne parasites such as the euglenozoan *Trypanosoma brucei* and the apicomplexan *Plasmodium* species, the causative agents of sleeping sickness and malaria, respectively, undergo massive crista remodeling as they alternate between mammalian hosts and insect vectors [36,37]. In both, cristae are absent from stages that steal nutrients from the host but emerge in stages that reside in the more austere midgut of insects.

Cristae remodeling also occurs due to stress. Upon starvation, the tubular cristae of the amoeba *Chaos carolinensis* are dramatically remodeled into an interconnected, paracrystalline morphology [31,32], a change proposed to mitigate oxidative stress [31]. Widening of cristae has been reported in hepatic cell lines during hypoxia [38], and cristae were reduced to stubby tubules upon inhibition of mitochondrial translation [29]. Viral infection of plants [39], fungi [40] and mammals [41] have also been associated with cristae deformations.

Cristae deformities have been correlated with aging and certain pathologies. During rapid aging of the fungus *Podospora anserina*, cristae disappear as the inner membrane splits into vesicles, partitioning the matrix [42]. During aging in mice and fruit flies, cristae tend to widen and, in extreme cases, low-density voids enveloped by inner membrane appear [30]. Cristae widening is a symptom of Leigh syndrome, a congenital neurometabolic disease often arising from mitochondrial DNA defects [43].

A notable instance of cristae remodeling occurs in animals during intrinsic apoptosis, which is triggered by the release of cytochrome c from mitochondria to the cytosol [44]. The bulk of cytochrome c trapped within cristae lumina is released when crista junctions and cristae widen upon induction of apoptosis, rendering the entire cytochrome c pool accessible to discharge from the organelle [8,45,46]. Thus, crista-junction diameter is an important parameter for cell viability. Treatment with the pro-apoptotic agonist tBID expands crista-junction diameter by 12–40 nm to a diameter exceeding the maximum reported crista-junction diameter (Figure S1C), supporting the theoretical role of crista junctions as diffusion barriers between the intermembrane space and crista lumen. However, cytochrome c release is independent of the inner membrane remodeling that occurs upon treatment with etoposide, another pro-apoptotic compound [47]. Interestingly this morphological change resembles the mitochondrial vesicularization seen during aging.

An Appraisal of Crista Diversity Throughout Eukaryotes

Armed with our crista-classification system (Figure 2), we mapped the ensuing morphotypes onto the current consensual tree of eukaryotes (Figure 3). Well-sampled eukaryotic groups, including opisthokonts, usually display significant variability in crista morphology, making reconstruction of their ancestral morphotype problematic. Some deep-branching and species-rich lineages, however, exhibit much more consistent crista morphologies (Figure S2). The expansive Stramenopiles-Alveolates-Rhizaria (SAR) supergroup almost exclusively contains tubulo-vesicular cristae. This uniformity in crista morphology is in sharp contrast to the profound diversity of the group, which contains various species-rich unicellular and multicellular lineages occupying numerous ecological niches (for example, diatoms, kelps, ciliates, and apicomplexans) [26]. Tubulo-vesicular cristae also predominate in the supergroup Amoebozoa, which contains diverse amoebae such as the slime mold *Dictyostelium discoideum*. Within the clade Discoba, the sister lineages

Parvulicifera sinerae; adapted from [146]. (F) Discoidal cristae of the heterolobosean *Stephanopogon pattersoni*; adapted from [147]. (G,H) Computer models generated from segmented three-dimensional tomograms of a mitochondrion in chick cerebellum. (G) The entire model showing all cristae in yellow, inner boundary membrane in light blue, and the outer membrane in dark blue. (H) Outer membrane, inner boundary membrane and four representative cristae in different colors. Adapted from [148]. This figure is inspired by [17].

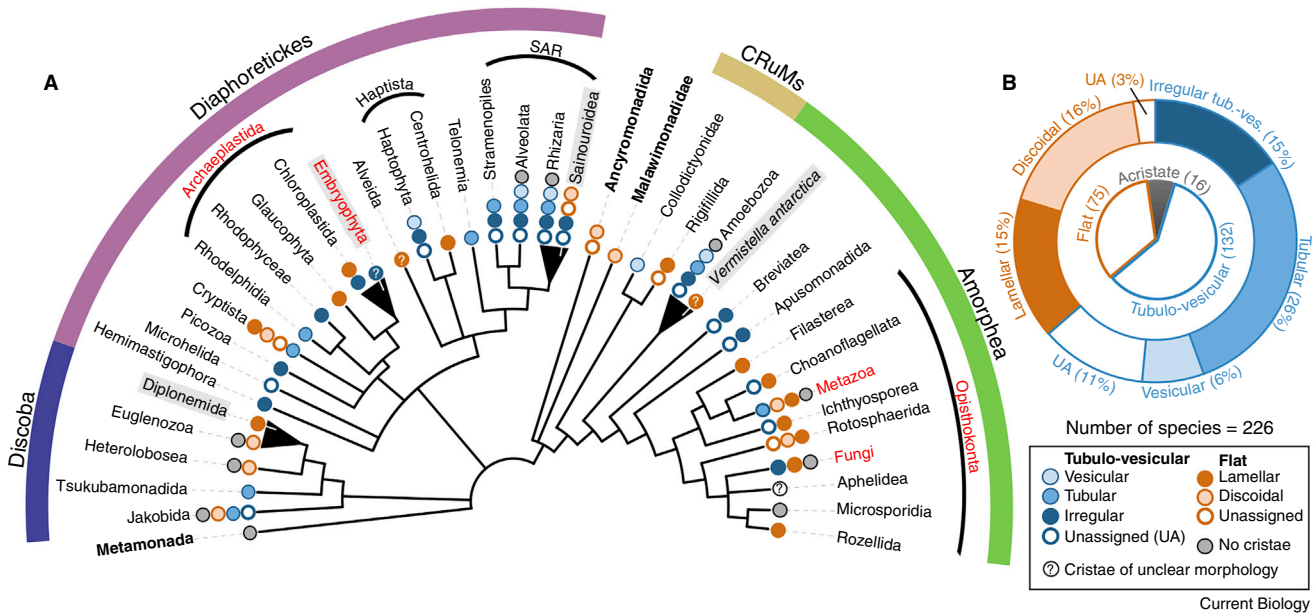


Figure 3. Distribution of crista morphotypes throughout eukaryotes.

(A) Distribution of morphotypes on a consensual phylogenetic tree of eukaryotes based on recently published phylogenomic analyses. Most-studied lineages, which include animals, fungi, and land plants (embryophyta) are in red. Grey shading indicates lineages that have considerably different crista morphotypes as compared to other representatives belonging to the same group (represented by the black triangles); in the case of Embryophyta, shading highlights a different morphology assigned to this group in this work in contrast to prevailing conjecture that they bear ‘lamellar’ cristae. (B) Overall abundance of crista morphotypes in eukaryotes. Descriptions of crista morphotypes from individual species sampled for this tree are given in Table S2. See also Figure S2.

Heterolobosea and Euglenozoa overwhelmingly and ancestrally have discoidal cristae. All four of these groups are among the most sampled in our study (Figure S2), giving credence to the attributed major crista morphotypes.

As is common in biology, each group that has a characteristic crista shape also has their own exceptions (Figure 3A). In the SAR supergroup, some representatives of Sainouroidea possess discoidal instead of tubulo-vesicular cristae [48]. *Vermistella antarctica* has flat, putatively lamellar cristae instead of the tubulo-vesicular ones seen in the rest of sampled amoebozoans [49]. Finally, abundant marine euglenozoans called diplomids also appear to have lamellar cristae [50] instead of the discoidal ones that prevail in Euglenozoa and Heterolobosea. These exceptions suggest that lamellar and discoidal cristae have been established several times independently. Comparative analysis of species within these groups may reveal molecular factors that underlie transition to lamellar or discoidal morphotypes and may also distinguish crista traits inherited from the last eukaryotic common ancestor from those that evolved convergently.

The clade Chloroplastida contains primarily photosynthetic organisms including green algae and land plants (embryophytes). Although flat lamellar cristae is the prevailing morphotype in Chloroplastida, we and others [51] have observed that the cristae of some plants and green algae have an irregular appearance in cross-section and resemble (or even belong to) the irregular tubulo-vesicular morphotype (Table S2). This goes against the general view that plants have classical lamellar cristae [18]. Because this contradiction is still preliminary, a dedicated comprehensive study of cristae from plants and other Chloroplastida members is warranted.

Fungi and metazoans (supergroup Opisthokonta) exhibit pleomorphic cristae. Both flat and tubulo-vesicular morphologies have been observed, sometimes even simultaneously within a single mitochondrion [6,11,12,52–55]. Pleomorphism may be intrinsic to archetypal lamellar cristae found in these organisms, an idea that we discuss further in the last section. This is also consistent with various crista morphologies observed in the unicellular relatives of the two groups (Table S2). However, the spectrum of crista morphotypes reported in opisthokonts may also reflect this group being the most thoroughly investigated among eukaryotes. Because cristae are dynamic, certain shapes may have gone undetected or been restricted to particular lineages (see examples in the Supplemental Information). Certainly, the giant amoeba *C. carolinensis* remodeling its ancestral tubular cristae into cubic crystalline lattice upon starvation argues that such dynamism is the case in the supergroup Amoebozoa. However, the tubulo-vesicular cristae overwhelmingly observed in the supergroup SAR are not likely to represent temporary forms, as this morphotype is observed in diverse members that occupy a variety of environments and exhibit various lifestyles.

How Crista-Shaping Molecules May Underlie Crista Diversity

Being composed of phospholipids and proteins, cristae are certainly shaped by variation in these molecules. We address this topic by comparing the biochemistry of the major molecular players that shape cristae and have been studied across taxa.

Cardiolipin

Although cristae of diverse eukaryotes assume different shapes, their membranes share topological features that require evolutionarily conserved molecules for their biogenesis. Among

these traits are negative curvature at crista junctions and positive curvature at crista rims [56,57]. Mitochondrial membranes from mammals, fungi, and plants have an overlapping phospholipid composition, with the quintessential mitochondrial phospholipid cardiolipin being less abundant compared to phosphatidylcholine and phosphatidylethanolamine [58]. However, the relatively greater inner-membrane enrichment of cardiolipin, as compared to phosphatidylcholine and phosphatidylethanolamine, indicates that cardiolipin is most relevant for crista shaping [58,59]. Cardiolipin and phosphatidylethanolamine are also concentrated at contact sites, which also overlap with crista junctions [60], albeit incompletely, as some contact sites have been observed away from cristae (Figure 1) [24,52].

Cardiolipin has a cone-like shape that is conducive for negative membrane curvature [61]. This is because the solute-facing, negatively charged head group is smaller than its bulkier glycerol backbone. Interestingly, various cardiolipin isoforms exist throughout eukaryotes that differ in the composition of their acyl chains, which represent the non-polar tails extending from the glycerol backbone [62] (Figure 4A,B). Cardiolipin polymorphism may thus be a factor in crista diversity. Additionally, cardiolipin facilitates respiratory-supercomplex assembly in opisthokonts [63–65], a process occurring on crista membranes [35,66]. It has also been proposed that cardiolipin is concentrated in the negative curvature at the interface between crista junctions and the inner boundary membrane [67], and that its enrichment on the matrix leaf of the inner membrane [58] may help to direct curvature so that the crista protrudes into the matrix.

An elegant experiment showed that the minimal requirement for crista-like structures *in vitro* is the presence of cardiolipin and acidic microdomains [68], since a tiny jet of acid induced tubular invaginations in phosphatidylcholine- and cardiolipin-containing liposomes. Importantly, this could not be reproduced when another negatively charged phospholipid replaced cardiolipin. Thus, cardiolipin has intrinsic membrane-bending properties that are induced by low pH, a condition present along the luminal face of the crista membrane due to the proton gradient that is generated by oxidative phosphorylation [9,25,66]. Furthermore, this study suggests that tubulo-vesicular cristae may represent the default morphotype, as the tubular shape has also been proposed for crista junctions [69].

Complex V Dimers

The link between crista form and function is exemplified by the membrane-bending activity of complex-V dimers, which are ultimately responsible for positive curvature at crista rims (Figure 1) [70,71]. Complex-V dimers from various taxa can assume one of four recently formalized configurations [70], which may underlie the aforementioned crista morphotypes. The dimerization of all these types is based on an interaction interface formed between two inner-membrane-integral F_O moieties and/or peripheral stalks, the latter running parallel to the central stalk that connects the F_O moiety and F_1 head (Figure 4C). Most complex-V dimer types are V-shaped, meaning that an angle originating from the interface of inner-membrane-embedded dimers eventually pries apart each monomer's F_1 head in the matrix [6,33,71,72]. These include the type-I dimers of opisthokonts and possibly land plants [6,72], type-II of green algae [71] and type-IV of euglenozoans [33]. The average angles between each monomer differ,

with the *Euglena* dimer being most acute (50°) and potato being the most obtuse (115°); the opisthokont F_1 heads are separated by $\sim 80^\circ$ (Figure 4C). In contrast, ciliates have U-shaped dimers designated type III, in which each F_1F_O monomer is erected in parallel [27]. Thus, this range of angles may induce different extents of positive curvature *in vivo*, perhaps contributing to crista diversity.

Complex-V dimers are in turn arranged to form an array. Type-I and type-II dimers, which mainly differ in the composition of their peripheral stalks [70], form straight, loosely packed rows that run along the crista edge [71,72]. Being perpendicular to the long axis of each dimer, the row appears to pucker positive curvature at the rims of cristae [71]. The dimer rows in the green alga *Polytomella* are more uneven, forming ridges that may underlie the irregular appearance of their tubulo-vesicular cristae in TEM [73].

The euglenozoan type-IV dimers form a closely packed lattice of interlaced rows, appearing as short ribbons that run slightly askew the crista edge [33]. This configuration arises from the offset peripheral stalks of type-IV dimers, not present in types I and II (Figure 4C). These different modes of V-shaped dimer row formation in opisthokont's type-I and euglenozoan's type-IV dimers may contribute to the different morphologies of lamellar and discoidal cristae, respectively.

Complex-V dimer rows directly impacting crista shape can be found in the tubular morphotype-bearing ciliates [27]. Whereas type-I dimers are planar, in a U-shaped type-IV dimer, each F_1 moiety is askew relative to each other when looking from the top (that is, the matrix side). This offset of the bulky F_1 heads in each dimer causes a twist within the row to accommodate the neighboring U-dimers, resulting in the long dimer row meandering as a right-handed helix. This ultimately shapes tubular crista morphology, which assumes a right-handed corkscrew appearance. Perhaps these U-shaped dimer rows are correlated with the apparent lack of acute positive membrane curvature, normally at crista edges, in tubular cristae anchored at each end to the inner boundary membrane by crista junctions.

In budding yeast, complex-V dimerization is mediated by subunits e and g, which are at the periphery of the F_O moiety [74]. Deletion of their corresponding genes results in unfolded cristae, giving mitochondria an onion-like appearance [53,72,75]. Both subunits facilitate the formation of ordered dimer rows and their ablation results in disordered distribution of F_1F_O monomers and thus cristae deformation [72]. Strikingly, this resembles deformities that arise upon dimer dissociation due to aging and disease [30,42,43]. Strangely, subunits e and g are not actually within the dimerization interface, so it is unclear by which mechanism they promote dimer formation [76]. However, it is likely that the proteins responsible for complex-V dimer formation in various taxa will be different given the variety of observed dimerization interfaces [70].

The inner-membrane-enriched phospholipid cardiolipin facilitates complex-V oligomerization in metazoans [64], consistent with the model that crista ridges formed by complex V serve as a proton sink for the lateral pH gradient adjacent to the crista membrane [6,9,70]. Cardiolipin may contribute to this model thanks to its two phosphate groups, which can trap single protons [77] (Figure 4A). Thus, the behavior of protein complexes, lipid content, and membrane shape all influence ATP generation on crista membranes.

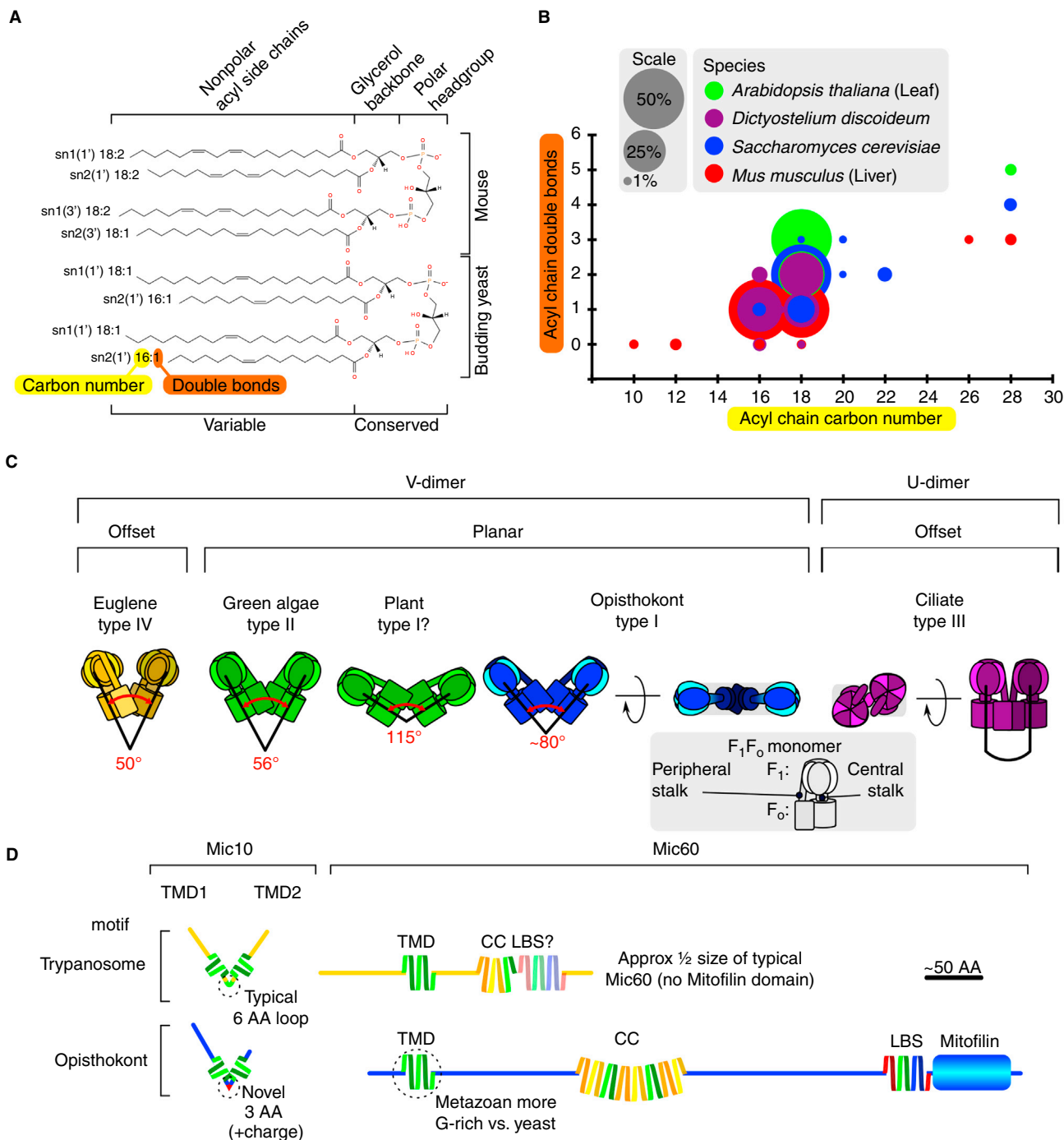


Figure 4. Crista-shaping molecules.

(A) Illustrative scheme of cardiolipin from mouse and budding yeast. Stereospecifically numbered (sn) head group positions of each side chain indicated on the right followed by their structure as indicated in colored highlights below. Structures were rendered using LIPID MAPS Cardiolipin Online Drawing Tool [149]. (B) Bubble chart summarizing cardiolipin side-chain diversity in four representative species. Color coding and size scale of each data point is shown in the key at the top. Each data point shows percentage of side chains that have a given acyl chain carbon number on the x-axis and double bonds on the y-axis. Data taken from Dataset S1 of [62]. (C) Survey of V- or U-dimer types of Complex V (F_1F_0 -ATP synthase) and angles between the F_1 -moiety heads in the former. Based on [27,33,71,72] using a recently established dimer classification system [70]. “?” indicates an interim assignment of dimer type. Grey inset, major structural features of the Complex-V monomer. (D) Domain architecture comparison of the two core MICOS subunits Mic10 and Mic60 from the euglenozoan *Trypanosoma brucei* and the opisthokont *Saccharomyces cerevisiae*. Hypothetical wedge shape depicted for Mic10 [115]. Putative lipid binding site (LBS) of trypanosome Mic60 indicated by faded icon and “?” [83, 98]. CC, coiled coil domain.

Current Biology

MICOS

The mitochondrial contact site and cristae organization system (MICOS) complex was originally discovered within the crista junctions of budding yeast [60,78,79], an organism in which MICOS has been the most researched [80,81]. The whole MICOS complex has been characterized in humans [82] and the euglenozoan *T. brucei* [83,84], and partially in the plant *Arabidopsis thaliana* [85]. Here, we discuss MICOS features conserved across these taxa that may conform crista shape to the crista-junction model, plus differences that may underlie crista diversity.

MICOS ablation is characterized by a substantial reduction in crista junctions and accumulation of elongated, detached cristae, often stacked alongside each other in the matrix. Interestingly, this phenotype is reduced by limiting the mitochondrial accumulation of the phospholipid phosphatidylethanolamine [86], hinting that it is perhaps needed for extending cristae. The archetypal role of MICOS in crista-junction formation and/or maintenance is highly conserved, confirmed in yeast [60,78,79,87–89], metazoans [90–94], and trypanosomes [83], thus spanning the ~1.8 billion years since the divergence of opisthokonts and euglenozoans [95].

Opisthokont MICOS contains six subunits in budding yeast and seven in animals. These subunits are organized into two inner-membrane-embedded subcomplexes centered around the core subunits Mic10 and Mic60 [89,92]. The Mic60 subcomplex also contains Mic19, the sole soluble intermembrane-space subunit. A Mic19 paralog named Mic25 is also found in human MICOS [18,96]. Mic19 interacts with the characteristic Mic60 mitofilin domain [18,89,97,98]. Mic19 may be critical for MICOS regulation because it is phosphorylated [99] and undergoes endoproteolytic cleavage in humans [96], neither of which occur in Mic25. In yeast, Mic19 was proposed to be a redox sensor due to the different oxidation states of its twin intramolecular disulfides [100]. Interestingly, Mic19 binding to the mitofilin domain, which modulates the intrinsic membrane remodeling activity of Mic60, is dependent on some of these disulfides [98].

The Mic10 subcomplex bends crista-junction membranes, shown in yeast to be mainly mediated by Mic10 oligomerization [56,101]. The Mic10 oligomer stability is oppositely affected by the yeast paralogs Mic26 and Mic27 [102]. These paralogs are bitopic, apolipoprotein O-like proteins [18,97] with evidence for cardiolipin interaction of one human paralog demonstrated by *in vitro* binding [103] and one paralog in yeast *in vivo* [89]. Cardiolipin is an appropriate phospholipid to sequester in crista junctions given its intrinsic negative curvature [61,67]. The Mic10 subcomplex also contains small, single-pass membrane proteins Mic12 (in yeast [104]) and Mic13 (in animals; also known as Qil1 [92,105]), which mediate coupling of the Mic10 and Mic60 sub-complexes. It remains an open question whether they are distant homologs, or analogs arising by convergent evolution [18,97]. Nevertheless, Mic13 appears to affect stability of all Mic10 subcomplex subunits, whereas Mic12 preferentially stabilizes Mic27. This difference may contribute to distinct MICOS stability and dynamics between metazoans and yeast.

The trypanosome MICOS complex has a different architecture. Six of its nine subunits are soluble intermembrane-space proteins, in contrast to the vast majority of opisthokont MICOS subunits being transmembrane proteins [83]. Furthermore,

trypanosome MICOS is divided vertically into inner-membrane-embedded and peripheral intermembrane-space sub-complexes, instead of the lateral arrangement of the aforementioned Mic10 and Mic60 sub-complexes [84]. The integral sub-complex appears to be organized around two Mic10 paralogs. It also contains a putative Mic60, which lacks the characteristic mitofilin domain but retains the rest of the domain architecture found in other Mic60 orthologs (Figure 4C) [19,83]. One of the soluble subunits was proposed to represent the missing mitofilin domain [83,84]. If true, this could explain the vertical arrangement of trypanosome MICOS, with subcomplexes being organized around Mic10 and a soluble mitofilin domain.

MICOS also facilitates the formation of contact sites between the inner and outer membranes. In opisthokonts and plants, Mic60 interacts with the translocase of the outer membrane (TOM) [79,85,106,107], a macromolecular complex through which nucleus-encoded proteins pass [108]. Furthermore, opisthokont and trypanosome MICOS both interact with the central β -barrel protein insertase Sam50 [60,83,94,106,107,109–112]. In humans, interaction with Sam50 is particularly stable, creating a >1 megadalton supercomplex called the ‘mitochondrial intermembrane space bridging complex’ [82,97,109,110]. This complex is specifically formed by the Sam50-Mic19-Mic60 axis, which is interrupted by the aforementioned Mic19 cleavage [96,111]. Uncleavable Mic25 participation in MICOS interaction with Sam50 [96] may explain the greater stability of the mitochondrial intermembrane-space bridging complex in humans as compared to yeast [82]. How trypanosome MICOS interacts with Sam50 remains unknown, especially given that mitofilin and Mic19 orthologs and/or analogs have not yet been identified.

Phospholipid exchange between the outer and inner membranes was proposed to occur at contact sites [58], which are enriched with phosphatidylethanolamine [59]. In yeast, MICOS brings an inner-membrane-embedded enzyme that converts phosphatidylserine to phosphatidylethanolamine in proximity to the outer membrane, allowing phosphatidylethanolamine synthesis in this membrane for eventual export into the endoplasmic reticulum [86]. Phosphatidylethanolamine export from *A. thaliana* mitochondria to the chloroplast relies on a MICOS–TOM tether [85]. Thus, MICOS has a conserved involvement in phospholipid trafficking and modification.

The close apposition of outer and inner membranes at contact sites is also conducive to protein import [108]. Indeed, MICOS interaction with the responsible protein machinery is a conserved feature. However, the details and degree of MICOS integration into various protein-import pathways appear to significantly differ among the examined taxa. In opisthokonts, MICOS interacts with one of two translocases of the inner membrane (TIM). MICOS in humans interacts with TIM22, which inserts polytopic proteins into the inner membrane, whereas in yeast it interacts with TIM23, which imports matrix-targeted proteins [113]. In yeast, the Mic60 mitofilin domain transiently interacts with Mia40, the central oxidoreductase catalyzing protein import into the intermembrane space [108], hypothetically to bring it in proximity to intermembrane-space precursors translocating through TOM [79]. In trypanosomes, a thioredoxin-like subunit named Mic20 appears to be directly involved in intermembrane-space protein import, perhaps replacing the missing Mia40 [83]. Mic20 depletion leads to aberrant cristae and

downregulation of intermembrane-space proteins, demonstrating the integration of organellar protein import and the shaping of crista membranes in trypanosomes. Perhaps the degree of MICOS integration into protein-import pathways may influence how and where proteins are inserted into crista membranes.

The core Mic10 and Mic60 subunits are ubiquitous, implying their presence in the last eukaryotic common ancestor [18,97]. Mic60 has a deeper origin, as some extant alphaproteobacteria contain its ortholog [3,18,97,114]. Their primacy for MICOS function is supported by observations that Mic10 and Mic60 ablation generally have more drastic impacts on crista morphology as compared to when other subunits are ablated [60,78,79,83,89,91]. Both subunits can remodel membranes *in vitro* [98,114,115], and their conservation seemingly negates their contribution to crista diversity. However, both core subunits have evolved novelties in different lineages that may yet be shown to promote diversity. All Mic10 homologs are comprised mostly of two conserved transmembrane domains and a small matrix-localized loop in between (Figure 4D) [101,115]. This may give Mic10 a wedge shape that is tapered toward the matrix, allowing their oligomers to cause negative curvature at crista junctions [115]. The matrix-side loop of opisthokonts is uniquely composed of three positively charged amino acids [83], which are required for proper insertion into the inner membrane [101]. Additionally, trypanosomes have two paralogs of Mic10; how they may contribute to discoidal cristae remains mysterious.

Aside from its characteristic mitofilin domain, Mic60 is poorly conserved [18] (Figure 4D). The Mic60 transmembrane domain is a constant structural feature [18], although it is glycine-rich in animals relative to yeast [45]. Consequently, animal Mic60 may diffuse more easily within membranes, making animal crista junctions more flexible for the remodeling needed for intrinsic apoptosis [8]. This difference may also underlie prevalence of slot-like and tubular crista junctions in yeast and animals, respectively.

In yeast, a fraction of Mic10 was shown to promote complex-V oligomerization [88,116], whereas these oligomers are destabilized by Mic60 [87]. Furthermore, cardiolipin-binding Mic27 interacts directly with complex V [117], whose oligomers are reinforced by cardiolipin [64]. Thus, there appears to be a complex interplay among these crista-shaping factors.

Opa1 and Mgm1

Two dynamin-related GTPases named Mgm1 and Opa1, found in fungi and metazoans, respectively, appear to be restricted to Opisthokonta [19]. Despite sharing many common properties, critical differences between Mgm1 and Opa1 may underlie some of the observed disparities between fungal and metazoan cristae, such as crista-junction morphology.

Mgm1 and Opa1 play central roles in mitochondrial fusion, merging the two inner membranes originating from each of the juxtaposed organelles into one [118,119]. They are both also endoproteolytically cleaved into long (l-Opa1; l-Mgm1) and short (s-Opa1; s-Mgm1) forms [120–125]. Each long form contains an amino-terminal transmembrane domain that anchors the intermembrane-space extruded protein into the inner membrane. Proteolytic cleavage downstream of the transmembrane domain releases the soluble short form into the intermembrane space. L-Opa1 and s-Opa1 together form oligomers *in vivo*

[46], whereas s-Mgm1 oligomers were shown to directly bind and remodel membranes *in vitro* [126]. S-Mgm1 tetramers can form stable helical filaments on negatively curved membranes inside lipid tubes, which resemble the lumen enclosed by cristae and crista junctions. Mgm1's GTPase activity induces conformational changes that can either expand or constrict the volume encompassed by the membrane. This mechanism of Mgm1 action can certainly inform the mechanism of crista-junction constriction by l-Opa1–s-Opa1 oligomers, which sequester cytochrome *c* within the crista lumen [46]. These Opa1 oligomers are disassembled upon stimulation with proapoptotic factors like tBID [45,46,57]. L-Opa1 has been shown to be particularly important for crista membrane remodeling [127], although this result has been contradicted by a report that crista junctions are unaffected by l-Opa1 loss [29].

Interestingly, the remodeling of crista membranes by Opa1 impacts respiratory-chain supercomplex formation [35] and complex-V oligomerization [128]. The latter phenomenon is not because Opa1 and complex V interact, but because membrane curvature influences row formation by complex V [70,71]. Additionally, Opa1 interacts with Mic60 [45,117,129] and associates with Mic10 [113], consistent with their respective roles in maintaining crista junctions. Opa1 is epistatic to Mic60 in controlling crista-junction stability, with the latter protein being disassembled from a complex also containing Mic19, and perhaps the rest of MICOS, upon crista-junction widening during apoptosis [45].

The uncanny similarity of Mgm1 and Opa1 ostensibly suggests that they are orthologs within the opisthokont lineage, and the literature frequently refers to them as such (for example [53,126]). However, their monophyly has been challenged [18]. Two critical differences between them argue for their independent evolutionary origin. First, they are processed by different mitochondrial proteases — Mgm1 is cleaved at a single site by mitochondrial rhomboid protease [130], whereas l-Opa1 is processed at two cleavage sites (S1 and S2) by several proteases. The zinc metalloprotease Oma1 is responsible for S1 cleavage [123–125,131], whereas the intermembrane-space-facing, inner membrane-embedded *i*-AAA protease processes S2 [121,125,132]. Significantly, when Opa1 is exogenously expressed in yeast, it is processed by the endogenous *m*-AAA and not rhomboid protease [133], further supporting the evolutionary divergence of the two GTPases.

Moreover, the Opa1 ablation phenotype differs from that of Mgm1. Opa1 downregulation results in widening of the crista lumen [45,46,57], whereas Mgm1 deletion results in the loss and emergence of lamellar and tubular cristae, respectively [53,134]. Technical differences in how these two proteins were depleted can only go so far to explain such distinct phenotypes. Given that yeast and metazoan crista junctions have slot-like and tubular morphologies, respectively, Mgm1 and Opa1 may be dynamin-like GTPases that act differently on cristae. Further work is needed to determine whether these differences reflect the possibility of different origins.

What Does Returning to the Fold Tell Us?

At first, crista shape may seem to be a rather superficial topic. However, as with other ancient and widespread eukaryotic structures, an exploration of crista diversity can lead to the identification of commonalities, allowing us to propose the existence

of fundamental biological properties that have persisted since they were inherited from the last eukaryotic common ancestor [95,135,136]. Furthermore, cristae shape is currently the only characteristic that can be used for comparative analyses across eukaryotes, given that in-depth molecular studies of cristae have been performed in only a handful of mostly opisthokont models. Because crista shape is a product of various molecules that play important roles in mitochondria, it represents an initial — and often sole — indication of the physiological state and function of mitochondria in diverse eukaryotes. Thus, we hope this review will stimulate more research into understudied protists using the crista classification system proposed here as a guide. Such research can in turn illuminate how mitochondria are integrated in various cellular milieus.

While the ‘omics’ age has deposed crista morphology as a viable phylogenetic character, some useful generalizations can be made about cristae by exploring their diversity. One is that tubulo-vesicular cristae likely represent the default crista morphotype. This is based not only on the wide distribution and relative preponderance of this morphotype in our extensive dataset (Figure 4A,B), but also by their simple tubular design, which can be recapitulated *in vitro* by the behavior of cardiolipin exposed to a pH gradient [68] or by crista-shaping proteins [98,114,115,126].

Another notion is that opisthokont lamellar cristae are likely an agglomeration of fused tubular cristae. Researchers have proposed this hypothesis to explain the observation that lamellar cristae are attached to the inner-boundary membrane by multiple crista junctions, whereas tubular cristae often have one crista junction [6,24,137]. In budding yeast, lamellar and tubular cristae co-exist, with the former being more abundant [53]. Interestingly, this balance is tipped in favor of tubulo-vesicular cristae when the membrane-remodeling factor Mgm1 is ablated. Recently, cristae fusion has been observed in human mitochondria, although it was not determined whether these were tubulo-vesicular cristae coalescing into the lamellar form [138]. Thus, a quorum of data is amassing to support the interpretation that several tubulo-vesicular cristae constitute the lamellar morphotype. Investigation of apparent lamellar cristae in non-opisthokont lineages may reveal that they too are fusions of single crista-junction morphotypes. For example, do discoidal cristae fuse to form the lamellar ones observed in diplomonids [50]? Do other cristae morphotypes fuse as well?

Individual cristae have been observed to contact each other via small contacts that are reminiscent of the crista junctions at their base [6,139]. Furthermore, tubular cristae are sometimes branched [140–142], perhaps a product of fusion between them. Are these inter-cristae contact points actually modified crista junctions, given that they too represent constrictions? And if yes, do they constitute diffusion barriers? Do the molecules that decorate crista junctions also localize to these contact points? Although these are not completely analogous to crista junctions, as they are not in proximity to outer membrane, they may still have an overlapping composition. Interestingly, over-expression of Mic10 or Mic60 in yeast promotes branched cristae [87,101], consistent with the hypothesis that at least some crista-junction-biogenesis factors may also have a role in these inter-cristae contact points.

A related question that arises here is how crista junctions affect crista function. Some opisthokont lamellar cristae have

multiple tubular crista junctions, whereas others are connected to the inner boundary membrane by a single slot-like crista junction. Although the concept of tubular crista junctions as diffusion barriers is straightforward, can the same be said of 100–300 nm-long slot-like crista junctions (Figure 1) [6,28]? Also, can the unconstricted crista junctions observed in *Paramecium* [27] be diffusion barriers, and are such crista junctions more widely distributed? Perhaps this is a general feature of tubular cristae that bear two crista junctions, and by defying the crista-junction model of basic crista architecture, they may represent a crista morphotype with bioenergetic properties that differ from those that conform to the crista-junction model.

Dobzhansky coined the famous adage that “nothing in biology makes sense except in the light of evolution” [143], and we encourage mitochondrial biologists working with canonical opisthokont models to also keep in mind the ‘dark matter’ of eukaryotes when considering their own work. Perhaps the lamellar cristae that adorn their favorite organisms are, in the end, unusual among eukaryotes. The physiological upshot of these types of cristae remains an open question, the answer to which may be one vital piece of our evolutionary history.

SUPPLEMENTAL INFORMATION

Supplemental Information can be found online at <https://doi.org/10.1016/j.cub.2020.02.053>.

ACKNOWLEDGEMENTS

This review is dedicated to the memory of Prof. Jiří Vávra (1932–2018), a wonderful scientist and educator who inspired protistologists worldwide. We thank Tomáš Bílý and Ondřej Gahura (Institute of Parasitology) for assistance with electron tomography pictures and critical reading of the text, respectively, and anonymous reviewers for helpful comments. Czech Science Foundation grants 20-23513S, 20-07186S and 17-21409S, ERC CZ grant LL1601, Czech Ministry of Education OPVVV16_019/0000759 and Czech Biolmaging grant LM2015062 supported this work.

REFERENCES

- Martijn, J., Vosseberg, J., Guy, L., Offre, P., and Ettema, T.J.G. (2018). Deep mitochondrial origin outside the sampled alphaproteobacteria. *Nature* 557, 101–105.
- Eme, L., Spang, A., Lombard, J., Stairs, C.W., and Ettema, T.J.G. (2017). Archaea and the origin of eukaryotes. *Nat. Rev. Microbiol.* 15, 711–723.
- Muñoz-Gomez, S.A., Wideman, J.G., Roger, A.J., and Slamovits, C.H. (2017). The origin of mitochondrial cristae from alphaproteobacteria. *Mol. Biol. Evol.* 34, 943–956.
- Wilkens, V., Kohl, W., and Busch, K. (2013). Restricted diffusion of OXPHOS complexes in dynamic mitochondria delays their exchange between cristae and engenders a transitory mosaic distribution. *J. Cell Sci.* 126, 103–116.
- Vogel, F., Bornhovd, C., Neupert, W., and Reichert, A.S. (2006). Dynamic subcompartmentalization of the mitochondrial inner membrane. *J. Cell Biol.* 175, 237–247.
- Davies, K.M., Strauss, M., Daum, B., Kief, J.H., Osiewacz, H.D., Rycovska, A., Zickermann, V., and Kühlbrandt, W. (2011). Macromolecular organization of ATP synthase and complex I in whole mitochondria. *Proc. Natl. Acad. Sci. USA* 108, 14121–14126.
- Gilkerson, R.W., Selker, J.M., and Capaldi, R.A. (2003). The cristal membrane of mitochondria is the principal site of oxidative phosphorylation. *FEBS Lett.* 546, 355–358.

8. Scorrano, L., Ashiya, M., Buttle, K., Weiler, S., Oakes, S.A., Mannella, C.A., and Korsmeyer, S.J. (2002). A distinct pathway remodels mitochondrial cristae and mobilizes cytochrome c during apoptosis. *Dev. Cell* 2, 55–67.
9. Rieger, B., Junge, W., and Busch, K.B. (2014). Lateral pH gradient between OXPHOS complex IV and F₀F₁ ATP-synthase in folded mitochondrial membranes. *Nat. Commun.* 5, 3103.
10. Stehling, O., and Lill, R. (2013). The role of mitochondria in cellular iron-sulfur protein biogenesis: mechanisms, connected processes, and diseases. *Cold Spring Harb. Perspect. Med.* 3, 1–17.
11. Zick, M., Rabl, R., and Reichert, A.S. (2009). Cristae formation-linking ultrastructure and function of mitochondria. *Biochim. Biophys. Acta* 1793, 5–19.
12. Vafai, S.B., and Mootha, V.K. (2012). Mitochondrial disorders as windows into an ancient organelle. *Nature* 491, 374–383.
13. Taylor, F.J.R. (1976). Flagellate phylogeny: A study in conflicts. *J. Protozool.* 23, 28–40.
14. Cavalier-Smith, T. (1997). Amoeboflagellates and mitochondrial cristae in eukaryote evolution: megasystematics of the new protozoan subkingdoms eozoa and neozoa. *Arch. Protistenkd.* 147, 237–258.
15. Cavalier-Smith, T. (1999). Zooflagellate phylogeny and the systematics of protozoa. *Biol. Bull.* 196, 393–396.
16. Patterson, D.J. (1999). The diversity of eukaryotes. *Am. Nat.* 154, 96–124.
17. Seravin, L.N. (1993). The basic types and forms of the fine structure of mitochondrial cristae: the degree of their evolutionary stability (capacity for morphological transformations). *Tsitologiia* 35, 3–34.
18. Muñoz-Gómez, S.A., Slamovits, C.H., Dacks, J.B., Baier, K.A., Spencer, K.D., and Wideman, J.G. (2015). Ancient homology of the mitochondrial contact site and cristae organizing system points to an endosymbiotic origin of mitochondrial cristae. *Curr. Biol.* 25, 1489–1495.
19. Muñoz-Gómez, S.A., Slamovits, C.H., Dacks, J.B., and Wideman, J.G. (2015). The evolution of MICOS: Ancestral and derived functions and interactions. *Commun. Integr. Biol.* 8, e1094593.
20. Palade, G.E. (1953). An electron microscope study of the mitochondrial structure. *J. Histochem. Cytochem.* 1, 188–211.
21. Sjöstrand, F.S. (1956). The ultrastructure of cells as revealed by the electron microscope. *Int. Rev. Cytol.* 5, 455–533.
22. Mannella, C.A. (2006). Structure and dynamics of the mitochondrial inner membrane cristae. *Biochim. Biophys. Acta* 1763, 542–548.
23. Frey, T.G., Perkins, G.A., and Ellisman, M.H. (2006). Electron tomography of membrane-bound cellular organelles. *Annu. Rev. Biophys. Biomol. Struct.* 35, 199–224.
24. Perkins, G., Renken, C., Martone, M.E., Young, S.J., Ellisman, M., and Frey, T. (1997). Electron tomography of neuronal mitochondria: three-dimensional structure and organization of cristae and membrane contacts. *J. Struct. Biol.* 119, 260–272.
25. Mannella, C.A., Pfeiffer, D.R., Bradshaw, P.C., Moraru, I.I., Slepchenko, B., Loew, L.M., Hsieh, C.E., Buttle, K., and Marko, M. (2001). Topology of the mitochondrial inner membrane: dynamics and bioenergetic implications. *IUBMB Life* 52, 93–100.
26. Keeling, P.J., and Burki, F. (2019). Progress towards the tree of eukaryotes. *Curr. Biol.* 29, R808–R817.
27. Mühleip, A.W., Joos, F., Wigge, C., Frangakis, A.S., Kühlbrandt, W., and Davies, K.M. (2016). Helical arrays of U-shaped ATP synthase dimers form tubular cristae in ciliate mitochondria. *Proc. Natl. Acad. Sci. USA* 113, 8442–8447.
28. Perkins, G.A., Renken, C.W., van der Klei, I.J., Ellisman, M.H., Neupert, W., and Frey, T.G. (2001). Electron tomography of mitochondria after the arrest of protein import associated with Tom19 depletion. *Eur. J. Cell Biol.* 80, 139–150.
29. Richter, U., Ng, K.Y., Suomi, F., Marttinen, P., Turunen, T., Jackson, C., Suomalainen, A., Vihinen, H., Jokitalo, E., Nyman, T.A., *et al.* (2019). Mitochondrial stress response triggered by defects in protein synthesis quality control. *Life Sci. Alliance* 2, e201800219.
30. Brandt, T., Mourier, A., Tain, L.S., Partridge, L., Larsson, N.G., and Kühlbrandt, W. (2017). Changes of mitochondrial ultrastructure and function during ageing in mice and *Drosophila*. *eLife* 6, e24662.
31. Deng, Y., Marko, M., Buttle, K.F., Leith, A., Mieczkowski, M., and Mannella, C.A. (1999). Cubic membrane structure in amoeba (*Chaos carolinensis*) mitochondria determined by electron microscopic tomography. *J. Struct. Biol.* 127, 231–239.
32. Pappas, G.D., and Brandt, P.W. (1959). Mitochondria. 1. Fine structure of the complex patterns in the mitochondria of *Pelomyxa carolinensis* Wilson (*Chaos chaos* L.). *J. Biophys. Biochem. Cytol.* 6, 85–90.
33. Mühleip, A.W., Dewar, C.E., Schnauffer, A., Kühlbrandt, W., and Davies, K.M. (2017). *In situ* structure of trypanosomal ATP synthase dimer reveals a unique arrangement of catalytic subunits. *Proc. Natl. Acad. Sci. USA* 114, 992–997.
34. Hackenbrock, C.R. (1966). Ultrastructural bases for metabolically linked mechanical activity in mitochondria. I. Reversible ultrastructural changes with change in metabolic steady state in isolated liver mitochondria. *J. Cell Biol.* 30, 269–297.
35. Cogliati, S., Frezza, C., Soriano, M.E., Varanita, T., Quintana-Cabrera, R., Corrado, M., Cipolat, S., Costa, V., Casarin, A., Gomes, L.C., *et al.* (2013). Mitochondrial cristae shape determines respiratory chain supercomplexes assembly and respiratory efficiency. *Cell* 155, 160–171.
36. Vickerman, K. (1985). Developmental cycles and biology of pathogenic trypanosomes. *Br. Med. Bull.* 41, 105–114.
37. Sturm, A., Mollard, V., Cozijnsen, A., Goodman, C.D., and McFadden, G.I. (2015). Mitochondrial ATP synthase is dispensable in blood-stage *Plasmodium berghei* rodent malaria but essential in the mosquito phase. *Proc. Natl. Acad. Sci. USA* 112, 10216–10223.
38. Plecitiá-Hlavatá, L., Engstová, H., Alán, L., Špaček, T., Dlasková, A., Smolková, K., Špačková, J., Tauber, J., Strádalová, V., Malinský, J., *et al.* (2016). Hypoxic HepG2 cell adaptation decreases ATP synthase dimers and ATP production in inflated cristae by mitofilin down-regulation concomitant to MICOS clustering. *FASEB J.* 30, 1941–1957.
39. Otulak, K., Chouda, M., Bujarski, J., and Garbaczewska, G. (2015). The evidence of tobacco rattle virus impact on host plant organelles ultrastructure. *Micron* 70, 7–20.
40. Zhang, L., Fu, Y., Xie, J., Jiang, D., Li, G., and Yi, X. (2009). A novel virus that infecting hypovirulent strain XG36-1 of plant fungal pathogen *Sclerotinia sclerotiorum*. *Virology* 391, 6–96.
41. Yang, Y., Shi, R., Soomro, M.H., Hu, F., Du, F., and She, R. (2018). Hepatitis E virus induces hepatocyte apoptosis via mitochondrial pathway in Mongolian gerbils. *Front. Microbiol.* 9, 460.
42. Daum, B., Walter, A., Horst, A., Osiewacz, H.D., and Kühlbrandt, W. (2013). Age-dependent dissociation of ATP synthase dimers and loss of inner-membrane cristae in mitochondria. *Proc. Natl. Acad. Sci. USA* 110, 15301–15306.
43. Siegmund, S.E., Grassucci, R., Carter, S.D., Barca, E., Farino, Z.J., Juanola-Falgarona, M., Zhang, P., Tanji, K., Hirano, M., Schon, E.A., *et al.* (2018). Three-dimensional analysis of mitochondrial cristae ultrastructure in a patient with Leigh Syndrome by *in situ* cryoelectron tomography. *iScience* 6, 83–91.
44. Tait, S.W., and Green, D.R. (2010). Mitochondria and cell death: outer membrane permeabilization and beyond. *Nat. Rev. Mol. Cell Biol.* 11, 621–632.
45. Glytsou, C., Calvo, E., Cogliati, S., Mehrotra, A., Anastasia, I., Rigoni, G., Raimondi, A., Shintani, N., Loureiro, M., Vazquez, J., *et al.* (2016). Optic atrophy 1 is epistatic to the core MICOS component MIC60 in mitochondrial cristae shape control. *Cell Rep.* 17, 3024–3034.
46. Frezza, C., Cipolat, S., Martins de Brito, O., Micaroni, M., Bezoussenko, G.V., Rudka, T., Bartoli, D., Polishuck, R.S., Dhanil, N.N., De Strooper, B., *et al.* (2006). OPA1 controls apoptotic cristae remodeling independently from mitochondrial fusion. *Cell* 126, 177–189.

47. Sun, M.G., Williams, J., Munoz-Pinedo, C., Perkins, G.A., Brown, J.M., Ellisman, M.H., Green, D.R., and Frey, T.G. (2007). Correlated three-dimensional light and electron microscopy reveals transformation of mitochondria during apoptosis. *Nat. Cell Biol.* **9**, 1057–1065.
48. Schuler, G.A., Tice, A.K., Pearce, R.A., Foreman, E., Stone, J., Gammill, S., Willson, J.D., Reading, C., Silberman, J.D., and Brown, M.W. (2018). Phylogeny and classification of novel diversity in Sainouroidea (Cercaria, Rhizaria) sheds light on a highly diverse and divergent clade. *Protist* **169**, 853–874.
49. Moran, D.M., Anderson, O.R., Dennett, M.R., Caron, D.A., and Gast, R.J. (2007). A description of seven Antarctic marine Gymnamoebae including a new subspecies, two new species and a new genus: *Neoparamoeba aestuarina antarctica* n. subsp., *Platylamoeba oblongata* n. sp., *Platylamoeba contorta* n. sp. and *Vermistella antarctica* n. gen. n. sp. *J. Eukaryot. Microbiol.* **54**, 169–183.
50. Tashyreva, D., Prokopchuk, G., Votýpka, J., Yabuki, A., Horák, A., and Lukeš, J. (2018). Life cycle, ultrastructure, and phylogeny of new diplomonads and their endosymbiotic bacteria. *mBio* **9**, e02447–17.
51. Douce, R. (1985). *Mitochondria in Higher Plants: Structure, Function, and Biogenesis* (Orlando, FL: Academic Press).
52. Nicastro, D., Frangakis, A.S., Typke, D., and Baumeister, W. (2000). Cryo-electron tomography of neurospora mitochondria. *J. Struct. Biol.* **129**, 48–56.
53. Harner, M.E., Unger, A.K., Geerts, W.J., Mari, M., Izawa, T., Stenger, M., Geimer, S., Reggiori, F., Westermann, B., and Neupert, W. (2016). An evidence based hypothesis on the existence of two pathways of mitochondrial crista formation. *eLife* **5**, e18853.
54. Winslow, J.L., Hollenberg, M.J., and Lea, P.J. (1991). Resolution limit of serial sections for 3D reconstruction of tubular cristae in rat liver mitochondria. *J. Electron Microsc. Tech.* **18**, 241–248.
55. Hanaki, M., Tanaka, K., and Kashima, Y. (1985). Scanning electron microscopic study on mitochondrial cristae in the rat adrenal cortex. *Microscopy* **34**, 373–380.
56. Barbot, M., and Meinecke, M. (2016). Reconstitutions of mitochondrial inner membrane remodeling. *J. Struct. Biol.* **196**, 20–28.
57. Quintana-Cabrera, R., Mehrotra, A., Rigoni, G., and Soriano, M.E. (2018). Who and how in the regulation of mitochondrial cristae shape and function. *Biochem. Biophys. Res. Commun.* **500**, 94–101.
58. Horvath, S.E., and Daum, G. (2013). Lipids of mitochondria. *Prog. Lipid Res.* **52**, 590–614.
59. Simbeni, R., Pon, L., Zinser, E., Paltauf, F., and Daum, G. (1991). Mitochondrial membrane contact sites of yeast. Characterization of lipid components and possible involvement in intramitochondrial translocation of phospholipids. *J. Biol. Chem.* **266**, 10047–10049.
60. Harner, M., Körner, C., Walther, D., Mokranjac, D., Kaesmacher, J., Welsch, U., Griffith, J., Mann, M., Reggiori, F., and Neupert, W. (2011). The mitochondrial contact site complex, a determinant of mitochondrial architecture. *EMBO J.* **30**, 4356–4370.
61. Jouhet, J. (2013). Importance of the hexagonal lipid phase in biological membrane organization. *Front. Plant Sci.* **4**, 494.
62. Oemer, G., Lackner, K., Muigg, K., Krumschnabel, G., Watschinger, K., Sailer, S., Lindner, H., Gnaiger, E., Wortmann, S.B., Werner, E.R., et al. (2018). Molecular structural diversity of mitochondrial cardiolipins. *Proc. Natl. Acad. Sci. USA* **115**, 4158–4163.
63. Böttinger, L., Horvath, S.E., Kleinschroth, T., Hunte, C., Daum, G., Pfanner, N., and Becker, T. (2012). Phosphatidylethanolamine and cardiolipin differentially affect the stability of mitochondrial respiratory chain super-complexes. *J. Mol. Biol.* **423**, 677–686.
64. Acehan, D., Malhotra, A., Xu, Y., Ren, M., Stokes, D.L., and Schlame, M. (2011). Cardiolipin affects the supramolecular organization of ATP synthase in mitochondria. *Biophys. J.* **100**, 2184–2192.
65. Dudek, J., Cheng, I.F., Balleiningner, M., Vaz, F.M., Streckfuss-Bomeke, K., Hubscher, D., Vukotic, M., Wanders, R.J., Rehling, P., and Guan, K. (2013). Cardiolipin deficiency affects respiratory chain function and organization in an induced pluripotent stem cell model of Barth syndrome. *Stem Cell Res.* **11**, 806–819.
66. Cogliati, S., Enriquez, J.A., and Scorrano, L. (2016). Mitochondrial cristae: where beauty meets functionality. *Trends Biochem. Sci.* **41**, 261–273.
67. Koob, S., and Reichert, A.S. (2014). Novel intracellular functions of apolipoproteins: the ApoO protein family as constituents of the Mitofilin/MINOS complex determines cristae morphology in mitochondria. *Biol. Chem.* **395**, 285–296.
68. Khalifat, N., Puff, N., Bonneau, S., Fournier, J.B., and Angelova, M.I. (2008). Membrane deformation under local pH gradient: mimicking mitochondrial cristae dynamics. *Biophys. J.* **95**, 4924–4933.
69. Renken, C., Siragusa, G., Perkins, G., Washington, L., Nulton, J., Salamon, P., and Frey, T.G. (2002). A thermodynamic model describing the nature of the crista junction: a structural motif in the mitochondrion. *J. Struct. Biol.* **138**, 137–144.
70. Kühlbrandt, W. (2019). Structure and mechanisms of F-type ATP synthases. *Annu. Rev. Biochem.* **88**, 515–549.
71. Blum, T.B., Hahn, A., Meier, T., Davies, K.M., and Kühlbrandt, W. (2019). Dimers of mitochondrial ATP synthase induce membrane curvature and self-assemble into rows. *Proc. Natl. Acad. Sci. USA* **116**, 4250–4255.
72. Davies, K.M., Anselmi, C., Wittig, I., Faraldo-Gomez, J.D., and Kühlbrandt, W. (2012). Structure of the yeast F₁F₀-ATP synthase dimer and its role in shaping the mitochondrial cristae. *Proc. Natl. Acad. Sci. USA* **109**, 13602–13607.
73. Dudkina, N.V., Kouřil, R., Bultema, J.B., and Boekema, E.J. (2010). Imaging of organelles by electron microscopy reveals protein–protein interactions in mitochondria and chloroplasts. *FEBS Lett.* **584**, 2510–2515.
74. Arnold, I., Pfeiffer, K., Neupert, W., Stuart, R.A., and Schägger, H. (1998). Yeast mitochondrial F₁F₀-ATP synthase exists as a dimer: identification of three dimer-specific subunits. *EMBO J.* **17**, 7170–7178.
75. Paumard, P., Vaillier, J., Couly, B., Schaeffer, J., Soubannier, V., Mueller, D.M., Brethes, D., di Rago, J.P., and Velours, J. (2002). The ATP synthase is involved in generating mitochondrial cristae morphology. *EMBO J.* **21**, 221–230.
76. Guo, H., Bueler, S.A., and Rubinstein, J.L. (2017). Atomic model for the dimeric F₀ region of mitochondrial ATP synthase. *Science* **358**, 936–940.
77. Haines, T.H., and Dencher, N.A. (2002). Cardiolipin: a proton trap for oxidative phosphorylation. *FEBS Lett.* **528**, 35–39.
78. Hoppins, S., Collins, S.R., Cassidy-Stone, A., Hummel, E., Devay, R.M., Lackner, L.L., Westermann, B., Schuldiner, M., Weissman, J.S., and Nunnari, J. (2011). A mitochondrial-focused genetic interaction map reveals a scaffold-like complex required for inner membrane organization in mitochondria. *J. Cell Biol.* **195**, 323–340.
79. von der Malsburg, K., Muller, J.M., Bohnert, M., Oeljeklaus, S., Kwiatkowska, P., Becker, T., Loniewska-Lwowska, A., Wiese, S., Rao, S., Milenkovic, D., et al. (2011). Dual role of mitofilin in mitochondrial membrane organization and protein biogenesis. *Dev. Cell* **21**, 694–707.
80. Wollweber, F., von der Malsburg, K., and van der Laan, M. (2017). Mitochondrial contact site and cristae organizing system: A central player in membrane shaping and crosstalk. *Biochim. Biophys. Acta* **1864**, 1481–1489.
81. Rampelt, H., Zerbes, R.M., van der Laan, M., and Pfanner, N. (2017). Role of the mitochondrial contact site and cristae organizing system in membrane architecture and dynamics. *Biochim. Biophys. Acta* **1864**, 737–746.
82. Kozjak-Pavlovic, V. (2017). The MICOS complex of human mitochondria. *Cell Tissue Res.* **367**, 83–93.
83. Kurov, I., Vancová, M., Schimanski, B., Cadena, L.R., Heller, J., Bílý, T., Potěšil, D., Eichenberger, C., Bruce, H., Oeljeklaus, S., et al. (2018). The diverged trypanosome MICOS complex as a hub for mitochondrial cristae shaping and protein import. *Curr. Biol.* **28**, 3393–3407.

84. Eichenberger, C., Oeljeklaus, S., Bruggisser, J., Mani, J., Haenni, B., Kaurov, I., Niemann, M., Zuber, B., Lukeš, J., Hashimi, H., *et al.* (2019). The highly diverged trypanosomal MICOS complex is organized in a nonessential integral membrane and an essential peripheral module. *Mol. Microbiol.* *12*, 1731–1743.
85. Michaud, M., Gros, V., Tardif, M., Brugiére, S., Ferro, M., Prinz, W.A., Toulmay, A., Mathur, J., Wozny, M., Falconet, D., *et al.* (2016). AtMic60 is involved in plant mitochondria lipid trafficking and is part of a large complex. *Curr. Biol.* *26*, 627–639.
86. Aaltonen, M.J., Friedman, J.R., Osman, C., Salin, B., di Rago, J.P., Nunnari, J., Langer, T., and Tatsuta, T. (2016). MICOS and phospholipid transfer by Ups2-Mdm35 organize membrane lipid synthesis in mitochondria. *J. Cell Biol.* *213*, 525–534.
87. Rabl, R., Soubannier, V., Scholz, R., Vogel, F., Mendl, N., Vasiljev-Neumeyer, A., Korner, C., Jagasia, R., Keil, T., Baumeister, W., *et al.* (2009). Formation of cristae and crista junctions in mitochondria depends on antagonism between Fcj1 and Su e/g. *J. Cell Biol.* *185*, 1047–1063.
88. Eydt, K., Davies, K.M., Behrendt, C., Wittig, I., and Reichert, A.S. (2017). Cristae architecture is determined by an interplay of the MICOS complex and the F₁F₀ ATP synthase via Mic27 and Mic10. *Microb. Cell* *4*, 259–272.
89. Friedman, J.R., Mourier, A., Yamada, J., McCaffery, J.M., and Nunnari, J. (2015). MICOS coordinates with respiratory complexes and lipids to establish mitochondrial inner membrane architecture. *eLife* *4*, e07739.
90. John, G.B., Shang, Y., Li, L., Renken, C., Mannella, C.A., Selker, J.M., Rangell, L., Bennett, M.J., and Zha, J. (2005). The mitochondrial inner membrane protein mitofilin controls cristae morphology. *Mol. Biol. Cell* *16*, 1543–1554.
91. Ott, C., Dorsch, E., Fraunholz, M., Straub, S., and Kozjak-Pavlovic, V. (2015). Detailed analysis of the human mitochondrial contact site complex indicate a hierarchy of subunits. *PLoS One* *10*, e0120213.
92. Guarani, V., McNeill, E.M., Paulo, J.A., Huttlin, E.L., Frohlich, F., Gygi, S.P., Van Vactor, D., and Harper, J.W. (2015). QIL1 is a novel mitochondrial protein required for MICOS complex stability and cristae morphology. *eLife* *4*, e06265.
93. Mun, J.Y., Lee, T.H., Kim, J.H., Yoo, B.H., Bahk, Y.Y., Koo, H.S., and Han, S.S. (2010). *Caenorhabditis elegans* mitofilin homologs control the morphology of mitochondrial cristae and influence reproduction and physiology. *J. Cell. Physiol.* *224*, 748–756.
94. Ding, C., Wu, Z., Huang, L., Wang, Y., Xue, J., Chen, S., Deng, Z., Wang, L., and Song, Z. (2015). Mitofilin and CHCHD6 physically interact with Sam50 to sustain cristae structure. *Sci. Rep.* *5*, 16064.
95. Betts, H.C., Puttick, M.N., Clark, J.W., Williams, T.A., Donoghue, P.C.J., and Pisani, D. (2018). Integrated genomic and fossil evidence illuminates life's early evolution and eukaryote origin. *Nat. Ecol. Evol.* *2*, 1556–1562.
96. Tang, J., Zhang, K., Dong, J., Yan, C., Hu, C., Ji, H., Chen, L., Chen, S., Zhao, H., and Song, Z. (2019). Sam50-Mic19-Mic60 axis determines mitochondrial cristae architecture by mediating mitochondrial outer and inner membrane contact. *Cell Death Differ* *27*, 146–160.
97. Huynen, M.A., Muhlmeister, M., Gotthardt, K., Guerrero-Castillo, S., and Brandt, U. (2016). Evolution and structural organization of the mitochondrial contact site (MICOS) complex and the mitochondrial intermembrane space bridging (MIB) complex. *Biochim. Biophys. Acta* *1863*, 91–101.
98. Hessenberger, M., Zerbes, R.M., Rampelt, H., Kunz, S., Xavier, A.H., Purfurst, B., Lillie, H., Pfanner, N., van der Laan, M., and Daumke, O. (2017). Regulated membrane remodeling by Mic60 controls formation of mitochondrial crista junctions. *Nat. Commun.* *8*, 15258.
99. Schauble, S., King, C.C., Darshi, M., Koller, A., Shah, K., and Taylor, S.S. (2007). Identification of ChChd3 as a novel substrate of the cAMP-dependent protein kinase (PKA) using an analog-sensitive catalytic subunit. *J. Biol. Chem.* *282*, 14952–14959.
100. Sakowska, P., Jans, D.C., Mohanraj, K., Riedel, D., Jakobs, S., and Chacinska, A. (2015). The oxidation status of Mic19 regulates MICOS assembly. *Mol. Cell Biol.* *35*, 4222–4237.
101. Bohnert, M., Zerbes, R.M., Davies, K.M., Mühleip, A.W., Rampelt, H., Horvath, S.E., Boenke, T., Kram, A., Perschil, I., Veenhuis, M., *et al.* (2015). Central role of Mic10 in the mitochondrial contact site and cristae organizing system. *Cell Metab.* *21*, 747–755.
102. Rampelt, H., Wollweber, F., Gerke, C., de Boer, R., van der Klei, I.J., Bohnert, M., Pfanner, N., and van der Laan, M. (2018). Assembly of the mitochondrial cristae organizer Mic10 is regulated by Mic26-Mic27 antagonism and cardiolipin. *J. Mol. Biol.* *430*, 1883–1890.
103. Weber, T.A., Koob, S., Heide, H., Wittig, I., Head, B., van der Blik, A., Brandt, U., Mittelbronn, M., and Reichert, A.S. (2013). APOOL is a cardiolipin-binding constituent of the Mitofilin/MINOS protein complex determining cristae morphology in mammalian mitochondria. *PLoS One* *8*, e63683.
104. Zerbes, R.M., Hoss, P., Pfanner, N., van der Laan, M., and Bohnert, M. (2016). Distinct roles of Mic12 and Mic27 in the mitochondrial contact site and cristae organizing system. *J. Mol. Biol.* *428*, 1485–1492.
105. Anand, R., Strecker, V., Urbach, J., Wittig, I., and Reichert, A.S. (2016). Mic13 is essential for formation of crista junctions in mammalian cells. *PLoS One* *11*, e0160258.
106. Zerbes, R.M., Bohnert, M., Stroud, D.A., von der Malsburg, K., Kram, A., Oeljeklaus, S., Warscheid, B., Becker, T., Wiedemann, N., Veenhuis, M., *et al.* (2012). Role of MINOS in mitochondrial membrane architecture: cristae morphology and outer membrane interactions differentially depend on mitofilin domains. *J. Mol. Biol.* *422*, 183–191.
107. Bohnert, M., Wenz, L.S., Zerbes, R.M., Horvath, S.E., Stroud, D.A., von der Malsburg, K., Muller, J.M., Oeljeklaus, S., Perschil, I., Warscheid, B., *et al.* (2012). Role of mitochondrial inner membrane organizing system in protein biogenesis of the mitochondrial outer membrane. *Mol. Biol. Cell* *23*, 3948–3956.
108. Wiedemann, N., and Pfanner, N. (2017). Mitochondrial machineries for protein import and assembly. *Annu. Rev. Biochem.* *86*, 685–714.
109. Ott, C., Ross, K., Straub, S., Thiede, B., Gotz, M., Goosmann, C., Krischke, M., Mueller, M.J., Krohne, G., Rudel, T., *et al.* (2012). Sam50 functions in mitochondrial intermembrane space bridging and biogenesis of respiratory complexes. *Mol. Cell Biol.* *32*, 1173–1188.
110. Xie, J., Marusich, M.F., Souda, P., Whitelegge, J., and Capaldi, R.A. (2007). The mitochondrial inner membrane protein mitofilin exists as a complex with SAM50, metaxins 1 and 2, coiled-coil-helix coiled-coil-helix domain-containing protein 3 and 6 and DnaJC11. *FEBS Lett.* *581*, 3545–3549.
111. Sastrri, M., Darshi, M., Mackey, M., Ramachandra, R., Ju, S., Phan, S., Adams, S., Stein, K., Douglas, C.R., Kim, J.J., *et al.* (2017). Sub-mitochondrial localization of the genetic-tagged mitochondrial intermembrane space-bridging components Mic19, Mic60 and Sam50. *J. Cell Sci.* *130*, 3248–3260.
112. Körner, C., Barrera, M., Dukanovic, J., Eydt, K., Harner, M., Rabl, R., Vogel, F., Rapaport, D., Neupert, W., and Reichert, A.S. (2012). The C-terminal domain of Fcj1 is required for formation of crista junctions and interacts with the TOB/SAM complex in mitochondria. *Mol. Biol. Cell* *23*, 2143–2155.
113. Callegari, S., Müller, T., Schulz, C., Lenz, C., Jans, D.C., Wissel, M., Opazo, F., Rizzoli, S.O., Jakobs, S., Urlaub, H., *et al.* (2019). A MICOS-TIM22 association promotes carrier import into human mitochondria. *J. Mol. Biol.* *431*, 2835–2851.
114. Tarasenko, D., Barbot, M., Jans, D.C., Kroppen, B., Sadowski, B., Heim, G., Mobius, W., Jakobs, S., and Meinecke, M. (2017). The MICOS component Mic60 displays a conserved membrane-bending activity that is necessary for normal cristae morphology. *J. Cell Biol.* *216*, 889–899.
115. Barbot, M., Jans, D.C., Schulz, C., Denkert, N., Kroppen, B., Hoppert, M., Jakobs, S., and Meinecke, M. (2015). Mic10 oligomerizes to bend mitochondrial inner membranes at cristae junctions. *Cell Metab.* *21*, 756–763.
116. Rampelt, H., Bohnert, M., Zerbes, R.M., Horvath, S.E., Warscheid, B., Pfanner, N., and van der Laan, M. (2017). Mic10, a core subunit of the mitochondrial contact site and cristae organizing system, interacts with the dimeric F₁F₀-ATP synthase. *J. Mol. Biol.* *429*, 1162–1170.

117. Schweppe, D.K., Chavez, J.D., Lee, C.F., Caudal, A., Kruse, S.E., Stupard, R., Marcinek, D.J., Shadel, G.S., Tian, R., and Bruce, J.E. (2017). Mitochondrial protein interactome elucidated by chemical cross-linking mass spectrometry. *Proc. Natl. Acad. Sci. USA* *114*, 1732–1737.
118. Meeusen, S., DeVay, R., Block, J., Cassidy-Stone, A., Wayson, S., McCaffery, J.M., and Nunnari, J. (2006). Mitochondrial inner-membrane fusion and crista maintenance requires the dynamin-related GTPase Mgm1. *Cell* *127*, 383–395.
119. Cipolat, S., de Brito, O.M., Dal Zilio, B., and Scorrano, L. (2004). OPA1 requires mitofusin 1 to promote mitochondrial fusion. *Proc. Natl. Acad. Sci. USA* *101*, 15927.
120. Herlan, M., Bornhovd, C., Hell, K., Neupert, W., and Reichert, A.S. (2004). Alternative topogenesis of Mgm1 and mitochondrial morphology depend on ATP and a functional import motor. *J. Cell Biol.* *165*, 167–173.
121. Song, Z., Chen, H., Fiket, M., Alexander, C., and Chan, D.C. (2007). OPA1 processing controls mitochondrial fusion and is regulated by mRNA splicing, membrane potential, and Yme1L. *J. Cell Biol.* *178*, 749–755.
122. Ishihara, N., Fujita, Y., Oka, T., and Mihara, K. (2006). Regulation of mitochondrial morphology through proteolytic cleavage of OPA1. *EMBO J.* *25*, 2966–2977.
123. Ehses, S., Raschke, I., Mancuso, G., Bernacchia, A., Geimer, S., Tondera, D., Martinou, J.C., Westermann, B., Rugarli, E.I., and Langer, T. (2009). Regulation of OPA1 processing and mitochondrial fusion by m-AAA protease isoenzymes and OMA1. *J. Cell Biol.* *187*, 1023–1036.
124. Head, B., Griparic, L., Amiri, M., Gandre-Babbe, S., and van der Bliek, A.M. (2009). Inducible proteolytic inactivation of OPA1 mediated by the OMA1 protease in mammalian cells. *J. Cell Biol.* *187*, 959–966.
125. Anand, R., Wai, T., Baker, M.J., Kladt, N., Schauss, A.C., Rugarli, E., and Langer, T. (2014). The i-AAA protease YME1L and OMA1 cleave OPA1 to balance mitochondrial fusion and fission. *J. Cell Biol.* *204*, 919–929.
126. Faelber, K., Dietrich, L., Noel, J.K., Wollweber, F., Pfützner, A.-K., Mühleip, A., Sánchez, R., Kudryashev, M., Chiaruttini, N., Lilie, H., et al. (2019). Structure and assembly of the mitochondrial membrane remodeling GTPase Mgm1. *Nature* *571*, 429–433.
127. Merkwirth, C., Dargazanli, S., Tatsuta, T., Geimer, S., Lower, B., Wunderlich, F.T., von Kleist-Retzow, J.C., Waisman, A., Westermann, B., and Langer, T. (2008). Prohibitins control cell proliferation and apoptosis by regulating OPA1-dependent cristae morphogenesis in mitochondria. *Genes Dev* *22*, 476–488.
128. Quintana-Cabrera, R., Quirin, C., Glytsou, C., Corrado, M., Urbani, A., Pellattiero, A., Calvo, E., Vazquez, J., Enriquez, J.A., Gerle, C., et al. (2018). The cristae modulator Optic atrophy 1 requires mitochondrial ATP synthase oligomers to safeguard mitochondrial function. *Nat. Commun.* *9*, 3399.
129. Barrera, M., Koob, S., Dikov, D., Vogel, F., and Reichert, A.S. (2016). OPA1 functionally interacts with MIC60 but is dispensable for crista junction formation. *FEBS Lett* *590*, 3309–3322.
130. Herlan, M., Vogel, F., Bornhovd, C., Neupert, W., and Reichert, A.S. (2003). Processing of Mgm1 by the rhomboid-type protease Pcp1 is required for maintenance of mitochondrial morphology and of mitochondrial DNA. *J. Biol. Chem.* *278*, 27781–27788.
131. Quirós, P.M., Ramsay, A.J., Sala, D., Fernández-Vizarrá, E., Rodríguez, F., Peinado, J.R., Fernández-García, M.S., Vega, J.A., Enriquez, J.A., Zorzano, A., et al. (2012). Loss of mitochondrial protease OMA1 alters processing of the GTPase OPA1 and causes obesity and defective thermogenesis in mice. *EMBO J* *31*, 2117–2133.
132. Stiburek, L., Česneková, J., Kostková, O., Fornůsková, D., Vinšová, K., Wenich, L., Houštěk, J., and Zeman, J. (2012). YME1L controls the accumulation of respiratory chain subunits and is required for apoptotic resistance, cristae morphogenesis, and cell proliferation. *Mol. Biol. Cell* *23*, 1010–1023.
133. Duvezin-Caubet, S., Koppen, M., Wagener, J., Zick, M., Israel, L., Bernacchia, A., Jagasia, R., Rugarli, E.I., Imhof, A., Neupert, W., et al. (2007). OPA1 processing reconstituted in yeast depends on the subunit composition of the m-AAA protease in mitochondria. *Mol. Biol. Cell* *18*, 3582–3590.
134. Amutha, B., Gordon, Donna M., Gu, Y., and Pain, D. (2004). A novel role of Mgm1p, a dynamin-related GTPase, in ATP synthase assembly and cristae formation/maintenance. *Biochem. J.* *381*, 19.
135. Lynch, M., Field, M.C., Goodson, H.V., Malik, H.S., Pereira-Leal, J.B., Roos, D.S., Turkewitz, A.P., and Sazer, S. (2014). Evolutionary cell biology: two origins, one objective. *Proc. Natl. Acad. Sci. USA* *111*, 16990–16994.
136. Richardson, E., Zerr, K., Tsaousis, A., Dorrell, R.G., and Dacks, J.B. (2015). Evolutionary cell biology: functional insight from "endless forms most beautiful". *Mol. Biol. Cell* *26*, 4532–4538.
137. Perkins, G.A., Renken, C.W., Frey, T.G., and Ellisman, M.H. (2001). Membrane architecture of mitochondria in neurons of the central nervous system. *J. Neurosci. Res.* *66*, 857–865.
138. Kondadi, A.K., Anand, R., Hänisch, S., Urbach, J., Zobel, T., Wolf, D.M., Segawa, M., Liesa, M., Shriihai, O.S., Weidtkamp-Peters, S., et al. (2020). Cristae undergo continuous cycles of membrane remodelling in a MICOS-dependent manner. *EMBO Rep.* *21*, e49776.
139. Perkins, G.A., Ellisman, M.H., and Fox, D.A. (2003). Three-dimensional analysis of mouse rod and cone mitochondrial cristae architecture: bioenergetic and functional implications. *Mol. Vis.* *9*, 60–73.
140. Mannella, C.A., Marko, M., Penczek, P., Barnard, D., and Frank, J. (1994). The internal compartmentation of rat-liver mitochondria: tomographic study using the high-voltage transmission electron microscope. *Microsc. Res. Tech.* *27*, 278–283.
141. Dyková, I., and Kostka, M. (2013). Illustrated Guide to Culture Collection of Free-living Amoebae (Prague: Academia).
142. Kudryavtsev, A., Wylezich, C., Schlegel, M., Walochnik, J., and Michel, R. (2009). Ultrastructure, SSU rRNA gene sequences and phylogenetic relationships of *Flamella* Schaeffer, 1926 (Amoebozoa), with description of three new species. *Protist* *160*, 21–40.
143. Dobzhansky, T. (1973). Nothing in biology makes sense except in the light of evolution. *Am. Biol. Teach.* *35*, 125–129.
144. Maier, I. (1997). The fine structure of the male gamete of *Ectocarpus siliculosus* (Ectocarpales, Phaeophyceae). I. General structure of the cell. *Eur. J. Phycol.* *32*, 241–253.
145. Finley, H.E., Brown, C.A., and Daniel, W.A. (1964). Electron microscopy of the ectoplasm and infraciliature of *Spirostomum ambiguum*. *J. Protozool.* *11*, 264–280.
146. Garcés, E., and Hoppenrath, M. (2010). Ultrastructure of the intracellular parasite *Parvilucifera sinerae* (Alveolata, Myzozoa) infecting the marine toxic planktonic dinoflagellate *Alexandrium minutum* (Dinophyceae). *Harmful Algae* *10*, 64–70.
147. Lee, W.J., Miller, K., and Simpson, A.G.B. (2014). Morphological and molecular characterization of a new species of *Stephanopogon*, *Stephanopogon pattersoni* n. sp. *J. Eukaryot. Microbiol.* *61*, 389–398.
148. Frey, T.G., and Mannella, C.A. (2000). The internal structure of mitochondria. *Trends Biochem. Sci.* *25*, 319–324.
149. Fahy, E., Sud, M., Cotter, D., and Subramaniam, S. (2007). LIPID MAPS online tools for lipid research. *Nucleic Acids Res.* *35*, W606–W612.